Impulsive correction to the elastic moduli obtained using the stress-fluctuation formalism in systems with truncated pair potential

H. Xu
LCP-A2MC, Institut Jean Barriol, Université de Lorraine & CNRS, 1 bd Arago, 57078 Metz Cedex 03, France

J. P. Wittmer,* P. Polińska, and J. Baschnagel
Institut Charles Sadron, Université de Strasbourg & CNRS, 23 rue du Loess, 67034 Strasbourg Cedex, France
(Received 1 August 2012; revised manuscript received 27 September 2012; published 31 October 2012)

The truncation of a pair potential at a distance r_c is well known to imply, in general, an impulsive correction to the pressure and other moments of the first derivatives of the potential. That, depending on r_c, the truncation may also be of relevance to higher derivatives is shown theoretically for the Born contributions to the elastic moduli obtained using the stress-fluctuation formalism in d dimensions. Focusing on isotropic liquids for which the shear modulus G must vanish by construction, the predicted corrections are tested numerically for binary mixtures and polydisperse Lennard-Jones beads in, respectively, $d = 3$ and 2 dimensions. Both models being glass formers, we comment briefly on the temperature (T) dependence of the (corrected) shear modulus $G(T)$ around the glass transition temperature T_g.

DOI: 10.1103/PhysRevE.86.046705 PACS number(s): 02.70.−c, 61.20.Ja, 65.20.−w

I. INTRODUCTION

Background. It is common practice in computational condensed matter physics [1–3] to truncate a pair interaction potential $U(r)$, with r being the distance between two particles i and j, at a conveniently chosen cutoff r_c. This allows us to reduce the number of interactions to be computed, and energy or force calculations become $O(n)$ processes where n denotes the particle number. However, the truncation also introduces technical difficulties, e.g., instabilities in the numerical solution of differential equations as well studied, especially for the molecular dynamics (MD) method [1,4]. Let us label the interaction between two particles $i < j$ by an index l. For simplicity of the presentation and without restricting much in practice the generality of our results, we assume the following:

(i) the potential $U(r)$ is short ranged, i.e., that it decays within a few particle diameters;

(ii) it scales as $U(r) \equiv u(s)$ with the reduced dimensionless distance $s = r/\sigma_l$, where σ_l characterizes the length scale of the interaction l;

(iii) the same reduced cutoff $s_c = r_c/\sigma_l$ is set for all interactions l.

For instance, for monodisperse particles with constant diameter σ, as for the standard Lennard-Jones (LJ) potential [1],

$$u_{\rm LJ}(s) = 4\epsilon\left(\frac{1}{s^{12}} - \frac{1}{s^6}\right), \tag{1}$$

the scaling variable becomes $s = r/\sigma$ and the reduced cutoff $s_c = r_c/\sigma$. The effect of introducing s_c is to replace $u(s)$ by the truncated potential

$$u_t(s) = u(s)H(s_c - s), \tag{2}$$

with $H(s)$ being the Heaviside function [5]. Even if Eq. (2) is taken *by definition* as the new system Hamiltonian, it is well known that impulsive corrections at the cutoff have to be taken into account in general for the pressure P and other moments of the first derivatives of the potential [2]. These corrections can be avoided by considering a properly shifted potential [2]

$$u_s(s) = [u(s) - u(s_c)]\,H(s_c - s) \tag{3}$$

as emphasized also in Sec. II A.

Goal of presented work. In this paper, we wish to examine the consequences of Eq. (3) on quantities involving second (and higher) derivatives of the potential. For these quantities, the standard shifting of a truncated potential is shown to be insufficient in general to avoid impulsive corrections. We demonstrate here that this is particulary the case for the Born contribution $C_B^{\alpha\beta\gamma\delta}$ (defined in the following) to the elastic moduli computed using the stress-fluctuation formalism described in detail in the literature [6–19]. This should be of importance for the *precise* localization of the transition between different thermodynamic phases by means of the elastic moduli, especially for liquid/sol ($G = 0$) to solid ($G > 0$) transitions in network forming systems where the shear modulus G plays the role of an order parameter [20]. Examples of current experimental and computational interest include the glass transition of colloidal or polymer liquids [18,21–26], colloidal gels [27], hyperbranched polymer chains with sticky end groups [28], or bridged networks of telechelic polymers in water-oil emulsions [29,30].

Outline. The paper is organized as follows: After recapitulating in Sec. II A the known corrections for the pressure and similar first derivatives of the potential, the impulsive correction for the general Born contribution $C_B^{\alpha\beta\gamma\delta}$ is given in Sec. II B. We describe then in Sec. II C the corrections on the compression modulus K and the shear modulus G in isotropic systems. We comment on polydispersity effects and mixed potentials in Sec. II D. Our results are reexpressed in terms of the radial pair distribution function $g(s)$ in Sec. II E, which allows us to predict the asymptotic behavior for large s_c. Section III gives some technical details on the two numerical model systems [17,31,32] in $d = 3$ and 2 dimensions used to

*joachim.wittmer@ics-cnrs.unistra.fr

test our predictions. This test is described in Sec. IV. We focus there on the high-temperature liquid regime of both models where the shear modulus G must vanish [6,33] since this provides a clear reference point for verifying the predicted corrections. Our main results are summarized in Sec. V A and an outlook on related issues is given in Sec. V B. Since both numerical models considered are well-known glass formers, we comment briefly in Sec. V C on ongoing simulations [34] investigating the shear modulus $G(T)$ as a function of temperature T around the glass transition temperature T_g. Such a characterization is of considerable current interest due to the qualitatively different theoretical suggestions put forward by mode-coupling theory (MCT) predicting a discontinuous jump [21,23,25] and by replica theory [26] implying a continuous transition [22,24].

II. THEORETICAL PREDICTIONS

A. Reminder

Truncated potential. As usual, for pairwise additive interactions the mean pressure $P = P_{\rm id} + P_{\rm ex}$ may be obtained as the sum of the ideal kinetic contribution $P_{\rm id} = k_{\rm B}T\rho$ and the excess pressure contribution [1,2]

$$P_{\rm ex} = \langle \hat{P}_{\rm ex} \rangle = -\frac{1}{dV} \sum_l \langle s_l u_{\rm t}'(s_l) \rangle \tag{4}$$

with $\rho = n/V$ being the number density, n the particle number, V the d-dimensional volume, $\hat{P}_{\rm ex}$ the instantaneous pressure, and $\langle \ldots \rangle$ indicating the thermal average over the configuration ensemble. (A prime denotes a derivative of a function with respect to its argument.) By taking the derivative of the truncated potential

$$u_{\rm t}'(s) = u'(s)H(s_{\rm c} - s) - u(s)\delta(s - s_{\rm c}), \tag{5}$$

the excess pressure may be written as the sum $P_{\rm ex} = \tilde{P}_{\rm ex} + \Delta P_{\rm ex}$ of an uncorrected (bare) contribution $\tilde{P}_{\rm ex}$ and an impulsive correction $\Delta P_{\rm ex}$. The latter correction is obtained numerically from [2]

$$\begin{aligned} \Delta P_{\rm ex} &= \lim_{s \to s_{\rm c}^-} h_1(s) \text{with} \\ h_1(s) &\equiv \frac{1}{dV} \sum_l \langle s_l u(s_l)\, \delta(s_l - s) \rangle \end{aligned} \tag{6}$$

being a weighted histogram. In practice, the proper limit $s \to s_{\rm c}^-$ may be replaced by setting $s = s_{\rm c}$ in $h_1(s)$.

Shifted potential. The impulsive correction related to first derivatives of the truncated potential can be avoided by considering the shifted potential $u_{\rm s}(s)$ [Eq. (3)] since $u_{\rm s}'(s) = u'(s)H(s_{\rm c} - s)$. With this choice, *no* impulsive correction arises either for similar observables such as, e.g., moments of the instantaneous excess pressure tensor

$$\begin{aligned} \hat{P}_{\rm ex}^{\alpha\beta} &= -\frac{1}{V} \sum_l s_l^\alpha \frac{\partial u_{\rm s}(s_l)}{\partial s_l^\beta} \\ &= -\frac{1}{V} \sum_l s_l u_{\rm s}'(s_l)\, n_l^\alpha n_l^\beta, \end{aligned} \tag{7}$$

where s_l^α stands for the spatial component α of the reduced distance between the particles and $n_l^\alpha = s_l^\alpha / s_l$ for the corresponding component of the normalized distance vector. Greek letters are used for the spatial coordinates $\alpha, \beta, \gamma, \delta = 1, \ldots, d$. (Note that $\hat{P}_{\rm ex} = {\rm Tr}[\hat{P}_{\rm ex}^{\alpha\beta}]/d$.) Specifically, if the potential is shifted, all impulsive corrections are avoided for the excess pressure fluctuations

$$C_{\rm F}^{\alpha\beta\gamma\delta} \equiv -\beta V \left(\left\langle \hat{P}_{\rm ex}^{\alpha\beta} \hat{P}_{\rm ex}^{\gamma\delta} \right\rangle - \left\langle \hat{P}_{\rm ex}^{\alpha\beta} \right\rangle \left\langle \hat{P}_{\rm ex}^{\gamma\delta} \right\rangle \right) \tag{8}$$

($\beta \equiv 1/k_{\rm B}T$ being the inverse temperature), which give important contributions, especially for polymer-type liquids [18,19] and amorphous solids [13,16] to the elastic moduli computed using the stress-fluctuation formalism [2,12]. Please note that since the stress is a two-point correlation function between the particles of the system, $C_{\rm F}^{\alpha\beta\gamma\delta}$ contains also in general three- and four-point correlations.

B. Key point made

Correction to the Born term. Another important contribution to the elastic moduli is given by the Born term $C_{\rm B}^{\alpha\beta\gamma\delta}$, already mentioned in the Introduction [35]. Being a moment of the first and the second derivatives of the potential, it is defined as [2,7,12,16,18,32]

$$C_{\rm B}^{\alpha\beta\gamma\delta} = \frac{1}{V} \sum_l \left\langle \left[s_l^2 u_{\rm s}''(s_l) - s_l u_{\rm s}'(s_l) \right] n_l^\alpha n_l^\beta n_l^\gamma n_l^\delta \right\rangle \tag{9}$$

using the notations given above. For solids with well-defined reference positions and displacement fields, the Born contribution is known to describe the energy change due to an *affine* response to an imposed homogeneous strain [12,13,16,32]. Assuming now a truncated and shifted potential, the impulsive correction $\Delta C_{\rm B}^{\alpha\beta\gamma\delta}$ to $C_{\rm B}^{\alpha\beta\gamma\delta} = \tilde{C}_{\rm B}^{\alpha\beta\gamma\delta} + \Delta C_{\rm B}^{\alpha\beta\gamma\delta}$ is simply obtained using

$$u_{\rm s}''(s) = u''(s)H(s_{\rm c} - s) - u'(s)\delta(s - s_{\rm c}), \tag{10}$$

which yields

$$\begin{aligned} \Delta C_{\rm B}^{\alpha\beta\gamma\delta} &= -\lim_{s \to s_{\rm c}^-} h_2^{\alpha\beta\gamma\delta}(s) \text{ with} \\ h_2^{\alpha\beta\gamma\delta}(s) &\equiv \frac{1}{V} \sum_l \left\langle s_l^2 u'(s_l) n_l^\alpha n_l^\beta n_l^\gamma n_l^\delta\, \delta(s_l - s) \right\rangle. \end{aligned} \tag{11}$$

General impulsive corrections. More generally, one might consider a property

$$A = \frac{1}{V} \sum_l \langle f(s_l) u_{\rm s}^{(n)}(s_l) \rangle \tag{12}$$

with $f(s)$ being a specified function and (n) denoting the nth derivative of the shifted potential $u_{\rm s}(s)$. Let us further suppose that all potential derivatives up to the $(n-2)$th one do vanish at the cutoff $s_{\rm c}$. It thus follows that $A = \tilde{A} + \Delta A$ takes an impulsive correction

$$\begin{aligned} \Delta A &= -\lim_{s \to s_{\rm c}^-} h_n(s) \text{with} \\ h_n(s) &\equiv \frac{1}{V} \sum_l \langle f(s_l) u^{(n-1)}(s_l)\, \delta(s_l - s) \rangle \end{aligned} \tag{13}$$

being the relevant histogram.

Generalized shifting. Obviously, the original potential can not only be shifted by a constant $u(s_{\rm c})$, but by a polynomial

of s to make the first and arbitrarily high derivatives of the potential vanish at $s = s_c$. In this way, all impulsive corrections could be avoided in principle. Since discontinuous forces at the cutoff may cause problems in MD simulations, a number of studies use, e.g., a "shifted-force potential" where a linear term is added to the potential [1,4]. The difference between the original potential and the generalized shifted potential removing the cutoff discontinuities means, of course, that the computed properties deviate to some extent from the original model. Only if the generalized shifting is weak, one may recover the correct thermodynamic properties using a first-order perturbation scheme [1]. Since the (simply) shifted potential $u_s(s)$ [Eq. (3)] is anyway the most common choice in simulations [8–10,13–19,31,32], we restrict the presentation on this case and demonstrate how the impulsive correction associated to the nonvanishing $u_s'(s_c^-)$ can be computed.

C. Isotropic systems

Lamé coefficients. In order to show that the above mentioned impulsive corrections may be of relevance computationally, we focus now on homogeneous and isotropic systems. It is assumed that not only the material properties, but also the external load is isotropic, i.e., the mean imposed pressure tensor is given by [36]

$$\left\langle \hat{P}_{\rm ex}^{\alpha\beta} \right\rangle = P\, \delta_{\alpha\beta}. \tag{14}$$

The two elastic Lamé coefficients λ and μ [7] characterizing their elastic properties may then be computed numerically using [18,19]

$$\begin{aligned} \lambda &= \lambda_{\rm F} + \lambda_{\rm B}, \\ \mu - P_{\rm id} &= \mu_{\rm F} + \mu_{\rm B}, \end{aligned} \tag{15}$$

where the only contribution due to the kinetic energy of the particles is contained by the ideal gas pressure $P_{\rm id}$ indicated for μ [37]. The first contributions indicated on the right-hand side of Eq. (15) are the excess pressure fluctuation contributions $\lambda_{\rm F}$ and $\mu_{\rm F}$, which may be obtained from the general $C_{\rm F}^{\alpha\beta\gamma\delta}$ by setting, e.g., $\alpha = \beta = 1$ and $\gamma = \delta = 2$ for $\lambda_{\rm F}$ and $\alpha = \gamma = 1$ and $\beta = \delta = 2$ for $\mu_{\rm F}$ characterizing the shear stress fluctuations. The "Born-Lamé coefficients" [18]

$$\lambda_{\rm B} \equiv \mu_{\rm B} \equiv \frac{1}{d(d+2)V} \sum_l \left\langle s_l^2 u''(s_l) - s_l u'(s_l) \right\rangle \tag{16}$$

may be obtained from the general Born terms $C_{\rm B}^{\alpha\beta\gamma\delta}$ by setting, e.g., $\alpha = \gamma = 1$ and $\beta = \delta = 2$. The d-dependent prefactor stems from the assumed isotropy of the system and the mathematical formula [5]

$$\left\langle \left(n_l^\alpha n_l^\beta \right)^2 \right\rangle = \frac{1}{d(d+2)} (1 + 2\delta_{\alpha\beta}) \tag{17}$$

($\delta_{\alpha\beta}$ being the Kronecker symbol [5]) for the components of a unit vector in d dimensions pointing into arbitrary directions. Equation (11) implies then an impulsive correction

$$\begin{aligned} \Delta\lambda_{\rm B} = \Delta\mu_{\rm B} &= -\lim_{s \to s_c^-} h_2(s) \text{with} \\ h_2(s) &\equiv \frac{1}{d(d+2)V} \sum_l \left\langle s_l^2 u'(s_l)\, \delta(s_l - s) \right\rangle. \end{aligned} \tag{18}$$

The histogram $h_2(s)$ is called below the "weighted (radial) pair distribution function" since it is related to the standard radial pair distribution function $g(r)$ [33], as further discussed in Sec. II E.

Compression and shear modulus. Instead of using the Lamé coefficients it is from the experimental point of view more natural to characterize isotropic bodies using the compression modulus K and the shear modulus G. The latter moduli may be expressed as [7]

$$K = (\lambda + P) + \frac{2}{d} G, \tag{19}$$

$$G = \mu - P = \mu_{\rm B} + \mu_{\rm F} - P_{\rm ex} \tag{20}$$

with $P = P_{\rm id} + P_{\rm ex}$ being the total imposed mean pressure. We follow here the notation of Ref. [18] to emphasize the explicit pressure dependence, which is often (incorrectly) omitted as clearly pointed out by Birch [38] and Wallace [7]. Using symmetry considerations, Eq. (19) can be reformulated to a numerically more straightforward expression first stated (to our knowledge) by Rowlinson [1,6]:

$$K = P + \eta_{\rm B} - \eta_{\rm F}. \tag{21}$$

Here, the second term $\eta_{\rm B}$ stands for the so-called "hypervirial" [1]

$$\eta_{\rm B} \equiv \lambda_{\rm B} + \frac{2}{d}(\mu_{\rm B} - P_{\rm ex}) \tag{22}$$

$$= \frac{1}{d^2 V} \sum_l \left\langle s_l^2 u_s''(s_l) + s_l u_s'(s_l) \right\rangle \tag{23}$$

in agreement with Eqs. (4) and (16). The last term

$$\eta_{\rm F} \equiv (-\lambda_{\rm F}) + \frac{2}{d}(-\mu_{\rm F}) \tag{24}$$

$$= \beta V \left(\left\langle \hat{P}_{\rm ex}^2 \right\rangle - \langle \hat{P}_{\rm ex} \rangle^2 \right) \tag{25}$$

characterizes the fluctuation of the excess pressure $\hat{P}_{\rm ex}$. As one expects, kinetic elastic contributions terms do not enter explicitly for the shear modulus G in Eq. (20). (An ideal gas does not have a finite shear modulus.) Since only the Born contributions $\lambda_{\rm B} = \mu_{\rm B}$ or $\eta_{\rm B}$ require a cutoff correction, this implies $K = \tilde{K} + \Delta K$ and $G = \tilde{G} + \Delta G$ with $\tilde{K}$ and $\tilde{G}$ being the uncorrected (bare) moduli and

$$\Delta K = \Delta\lambda_{\rm B} + \frac{2}{d}\Delta\mu_{\rm B} = \frac{2+d}{d}\Delta\mu_{\rm B}, \tag{26}$$

$$\Delta G = \Delta\mu_{\rm B} \tag{27}$$

being the impulsive corrections. We shall test these predictions numerically in Sec. IV.

D. Polydispersity and mixed potentials

As stated in the Introduction, we assume throughout this work the scaling $U(r) \equiv u(s)$ of the pair potential in terms of the reduced distance $s = r/\sigma_l$. This is done not only for dimensional reasons but, more importantly, to describe a broad range of model systems for mixtures and polydisperse systems where σ_l may differ for each interaction l. Moreover, the type and/or the parameter set of the pair potential may vary for different interactions. For such mixed potentials $u(s)$, $u_t(s)$ and $u_s(s)$ and their derivatives take in principle an explicit

index l, i.e., one should write $u_l(s)$, $u_{t,l}(s)$, $u_{s,l}(s)$, and so on. This is not done here to keep a concise notation. For example, one might wish to consider the following:

(i) a generic polymer bead-spring model where some interactions l describe the bonding between monomers along the chain (which are normally not truncated and need not to be corrected) and the truncated excluded volume interactions between the monomers [19];

(ii) the generalization of the monodisperse LJ potential [Eq. (1)] to a mixture or polydisperse system with

$$u_l(s) = 4\epsilon_l(s^{-12} - s^{-6}) \text{ with } s = r/\sigma_l, \tag{28}$$

where ϵ_l and σ_l are fixed for each interaction l. In practice, each particle i may be characterized by an energy scale E_i and a "diameter" D_i. The interaction parameters $\epsilon_l(E_i, E_j)$ and $\sigma_l(D_i, D_j)$ are then given in terms of specified functions of these properties [32];

(iii) the extensively studied Kob-Andersen (KA) model for binary mixtures of beads of types A and B [31], a particular case of Eq. (28) with fixed interaction ranges σ_{AA}, σ_{BB}, and σ_{AB} and energy parameters ϵ_{AA}, ϵ_{BB}, and ϵ_{AB} characterizing, respectively, AA, BB, and AB contacts;

(iv) a network forming emulsion of oil droplets in water bridged by telechelic polymers where the oil droplets are modeled as big LJ spheres, the telechelic polymers by a bead-spring model with a soluble "spacer" in the middle of the chain, and insoluble end groups ("stickers") strongly attracted by the oil droplets [29,30]. Assuming sufficiently strong (in strength, number, and lifetime) sticker-oil interactions, such a system behaves as a soft solid with a finite shear modulus G (at least for a fixed finite sampling time), which may be probed, at least in principle, using Eq. (20).

The impulsive corrections given in Eq. (6) for the pressure P, in Eq. (11) for the general Born term $C_B^{\alpha\beta\gamma\delta}$, and in Eq. (18) for the Born-Lamé coefficients $\lambda_B = \mu_B$ have been stated in terms of, respectively, the weighted histograms $h_1(s)$, $h_2^{\alpha\beta\gamma\delta}(s)$, and $h_2(s)$. These expressions remain valid for explicitly l-dependent potentials and, from the numerical point of view, this is all that is needed. The direct computation of these histograms remains in all cases straightforward, as illustrated in Sec. IV A.

E. Radial pair distribution function $g(r)$

Notations. For isotropic systems, it is common practice to reexpress correlations and histograms in terms of the radial pair distribution function $g(r)$ [6,33]. This is also of interest here since for large cutoff distances, the pair distribution function must drop out, $g(r_c) \to 1$, allowing us thus to predict the corrections in this limit. Let us remind first that, using the Gamma function $\Gamma(x)$ [5], the $(d-1)$-dimensional surface of a d sphere of radius r is given by

$$A(r) = \frac{2\pi^{d/2}}{\Gamma(d/2)}\, r^{d-1} \text{ for } d = 2,3,\ldots \tag{29}$$

and similarly for the (dimensionless) surface $A(s)$ using the reduced distance s.

Monodisperse interactions. For strictly monodisperse particles and similar interactions of constant interaction range σ, it is seen that Eq. (6) for the pressure correction becomes

$$\Delta P_{ex} = \frac{1}{2}\,\frac{1}{d}\rho^2\sigma^d A(s_c) s_c u(s_c) g(s_c), \tag{30}$$

where the factor $1/2$ assures that every interaction is only counted once. For the LJ potential [Eq. (1)], this leads to

$$\Delta P_{ex} = -\frac{4\pi^{d/2}}{\Gamma(d/2)d}(\rho\sigma^d)^2\frac{\epsilon}{\sigma^d}s_c^{d-6}\left(1 - s_c^{-6}\right)g(s_c). \tag{31}$$

Please note that Eq. (3.2.7) given in Ref. [2] is recovered by setting $d = 3$ and assuming $g(s_c) \approx 1$. Similarly, one obtains from Eq. (18) the correction

$$\Delta\mu_B = -\frac{1}{2}\,\frac{1}{d(d+2)}\rho^2\sigma^d A(s_c) s_c^2 u'(s_c) g(s_c) \tag{32}$$

for the Born-Lamé coefficient. For a LJ potential, this becomes

$$\Delta\mu_B = -\frac{24\pi^{d/2}}{d(d+2)\Gamma(d/2)}(\rho\sigma^d)^2\frac{\epsilon}{\sigma^d} f_{LJ}(s_c) g(s_c), \tag{33}$$

where we have defined

$$f_{LJ}(s) \equiv [1 - (s_0/s)^6]/s^{6-d} \tag{34}$$

with $s_0 = 2^{1/6}$ being the minimum of the potential. Note that $\Delta\mu_B$ vanishes for $s \to s_0$. For sufficiently large cutoff distances where $g(s_c) \approx 1$, the correction decays as

$$\Delta\mu_B \sim -A(s_c) s_c^2 u'(s_c), \tag{35}$$

e.g., $\Delta\mu_B \sim -1/s_c^{6-d}$ for a LJ potential. (Only for $d < 6$ the cutoff correction vanishes in the large-s limit.) This asymptotic behavior also holds for the more complicated cases discussed in the following.

Mixtures. Many experimentally relevant systems have mixed potentials, such as the KA model for binary mixtures sketched above. In general, the interaction potential $U_{ab}(r) = u_{ab}(s)$ between beads of two species a and b takes different energy parameters, which causes different weights at the cutoff depending on which particles interact. The impulsive corrections of such mixtures are readily obtained by linear superposition of Eq. (32) for different contributions (a,b). Let $c_a = \rho_a/\rho$ denote the mole fraction of species a, σ_{ab} the interaction range between a bead of type a and a bead of type b, and $g_{ab}(s)$ the respective radial pair distribution function. The impulsive correction to the Born-Lamé coefficient thus becomes

$$\Delta\mu_B = -\frac{1}{2}\,\frac{1}{d(d+2)}\rho^2 A(s_c) s_c^2 \times \sum_a \sum_b c_a c_b \sigma_{ab}^d u'_{ab}(s_c)\, g_{ab}(s_c), \tag{36}$$

where we have used that for all types of interaction, we have the *same* reduced cutoff s_c.

Let us now assume a mixture described by the generalized LJ potential $u_{ab}(s) = 4\epsilon_{ab}(1/s^{12} - 1/s^6)$ with $s = r/\sigma_{ab}$. A reference energy ϵ_{ref} and a reference interaction range σ_{ref} may arbitrarily be defined using, say, the interaction of two beads of type $a = b = 1$, i.e., $\epsilon_{ref} \equiv \epsilon_{11}$ and $\sigma_{ref} \equiv \sigma_{11}$. Defining the dimensionless ratios $w_{ab} \equiv \epsilon_{ab}/\epsilon_{ref}$ and $v_{ab} = (\sigma_{ab}/\sigma_{ref})^d$, we

may thus rewrite the general Eq. (36) as

$$\Delta\mu_{\rm B} = -\frac{24\pi^{d/2}}{d(d+2)\Gamma(d/2)}\left(\rho\sigma_{\rm ref}^d\right)^2\frac{\epsilon_{\rm ref}}{\sigma_{\rm ref}^d}\ f_{\rm LJ}(s_{\rm c}) \times \sum_a\sum_b c_a c_b v_{ab} w_{ab}\ g_{ab}(s_{\rm c}). \quad (37)$$

Since $g_{ab}(s_{\rm c}) \to 1$ for large $s_{\rm c}$, the function $f_{\rm LJ}(s_{\rm c})$ determines the scaling as already stated above [Eq. (35)].

Continuous polydispersity. We turn now to systems with a continuous polydispersity as in the second model investigated numerically below. Let us assume that each bead is characterized by a bead diameter D which is distributed according to a well-defined normalized distribution c_t with $t = D/\sigma_{\rm ref}$ being a reduced bead diameter with respect to some reference length $\sigma_{\rm ref}$. To be specific, we shall assume a generalized LJ potential [Eq. (28)], where the interaction range $\sigma_{tt'}$ and the energy scale $\epsilon_{tt'}$ between two beads are uniquely specified by the two reduced diameters t and t'. Defining $w_{tt'} = \epsilon_{tt'}/\epsilon_{\rm ref}$, $v_{tt'} = (\sigma_{tt'}/\sigma_{\rm ref})^d$ and using the radial pair distribution function $g_{tt'}(s)$ for two beads of reduced diameter t and t', the double sum in Eq. (37) can be rewritten as the double integral

$$\Delta\mu_{\rm B} = -\frac{24\pi^{d/2}}{d(d+2)\Gamma(d/2)}\left(\rho\sigma_{\rm ref}^d\right)^2\frac{\epsilon_{\rm ref}}{\sigma_{\rm ref}^d}\ f_{\rm LJ}(s_{\rm c}) \times \int dt \int dt'\ c_t c_{t'} v_{tt'} w_{tt'}\ g_{tt'}(s_{\rm c}). \quad (38)$$

In order to determine $\Delta\mu_{\rm B}$ from Eq. (38), one needs to prescribe the laws for c_t, $\sigma_{tt'}$, and $\epsilon_{tt'}$. In the large-$s_{\rm c}$ limit, the double integral becomes in any case constant, i.e., we have again $\Delta\mu_{\rm B} \sim -f_{\rm LJ}(s_{\rm c}) \sim -1/s_{\rm c}^{6-d}$.

III. COMPUTATIONAL ISSUES

To illustrate the above predictions, we present computational data using two extremely well-studied models of simple liquids at high temperatures, which are described in detail elsewhere [17,31,32]:

(i) The already mentioned KA model [31] for binary mixtures of LJ beads in $d = 3$ has been investigated by means of Langevin MD simulation [2] imposing a temperature $T = 0.8$ for $n = n_{\rm A} + n_{\rm B} = 6912$ beads per simulation box, a total density $\rho = 1.0$, and molar fractions $c_a = n_{\rm A}/n = 0.8$ and $c_b = n_{\rm B}/n = 0.2$ for both types of beads A and B. As in Ref. [31], we set $\sigma_{\rm AA} = 1.0\sigma$, $\sigma_{\rm BB} = 0.88\sigma$, and $\sigma_{\rm AB} = 0.8\sigma$ for the interaction range and $\epsilon_{\rm AA} = 1.0\epsilon$, $\epsilon_{\rm BB} = 0.5\epsilon$, and $\epsilon_{\rm AB} = 1.5\epsilon$ for the LJ energy scales. Only data for the usual cutoff $s_{\rm c} = 2.5$ are presented.

(ii) Using Monte Carlo (MC) simulations [1,2], we have computed in $d = 2$ dimensions a specific case of the generalized LJ potential [Eq. (28)], where all interaction energies are identical, $\epsilon_l = \epsilon$, and the interaction range is set by the Lorentz rule $\sigma_l = (D_i + D_j)/2$ [33] with D_i and D_j being the diameters of the interacting particles. Following Ref. [32], the bead diameters of this polydisperse LJ (pLJ) model are uniformly distributed between 0.8σ and 1.2σ. For the examples reported in Sec. IV, we have used a temperature $T = 1.0$, $n = 10\,000$ beads per box, and a density $\rho \approx 0.72$.

We use LJ units throughout this work, and Boltzmann's constant $k_{\rm B}$ is set to unity. For the indicated parameter choices, both systems correspond to isotropic liquids. Table I summarizes various properties of the pLJ model for different reduced cutoff distances $s_{\rm c}/s_0$. Considering thermodynamic properties per particle (rather than per volume), we have made the data dimensionless by rescaling with inverse temperature β and density ρ. While we keep the temperature T constant for each model in Sec. IV, temperature effects are briefly commented on in Sec. V C given at the end of the paper.

TABLE I. Some properties of pLJ beads at temperature $T = 1$ and density $\rho \approx 0.72$ for several computed values of the reduced cutoff distance $s_{\rm c}/s_0$ with $s_0 = 2^{1/6}$ being the minimum of the potential: energy per bead e, total pressure $P = P_{\rm id} + P_{\rm ex}$, uncorrected compression modulus $\tilde{K}$, corrected compression modulus $K = \tilde{K} + 2\Delta\mu_{\rm B}$, bare shear modulus $\tilde{G}$, and impulsive correction $\Delta\mu_{\rm B}$ obtained from the histogram $h_2(s)$ at $s = s_{\rm c}$. The corrected shear modulus $G = \tilde{G} + \Delta G$ vanishes as it should. The last column refers to the compression modulus K obtained using Eq. (39) for isobaric ensembles kept at the same pressure P (third column).

$s_{\rm c}/s_0$	$e\beta$	$P\beta/\rho$	$\tilde{K}\beta/\rho$	$K\beta/\rho$	$\tilde{G}\beta/\rho$	$\Delta\mu_{\rm B}\beta/\rho$	$K\beta/\rho$
0.9	0.255	5.08	−20.4	17.7	−18.95	19.05	17.4
1.0	0.523	6.01	22.5	22.5	0.03	0.03	22.4
1.1	0.176	5.46	24.2	20.4	1.97	−1.92	20.6
1.5	−1.79	3.61	17.6	16.7	0.36	−0.43	16.8
2.0	−2.43	3.17	16.7	16.1	0.31	−0.32	16.0
2.5	−2.64	3.01	15.8	15.6	0.08	−0.10	15.7
3.0	−2.72	2.95	15.6	15.5	0.08	−0.06	15.5
3.5	−2.75	2.93	15.6	15.5	0.02	−0.03	15.3
4.0	−2.77	2.92	15.7	15.7	0.03	−0.02	15.5

IV. COMPUTATIONAL RESULTS

A. Weighted pair distribution function $h_2(s)$

The weighted radial pair distribution function $h_2(s)$ [Eq. (18)] is presented in Fig. 1. Several cutoff distances $s_{\rm c}$ are given for the pLJ model, but for clarity only for distances $s \leqslant s_{\rm c}$. For the KA model, only one cutoff is given, but this also for $s > s_{\rm c}$. Note that albeit different $s_{\rm c}$ for each model correspond strictly speaking to different state points, as better seen from the energies per particle e or total pressures P indicated in Table I, the histograms vary only weakly with $s_{\rm c}$. Strong differences become only apparent for very small $s_{\rm c}$ as shown for $s_{\rm c} = 0.9s_0$ in the inset. One can thus use the histogram obtained for one $s_{\rm c}$ to anticipate the impulsive correction for a different cutoff. Note that for large distances corresponding to an attractive interaction, we have $h_2(s) > 0$ (main panel). Obviously, $h_2(s)$ vanishes at the minimum of the potential $s = s_0$ and for very large distances s. Since $g(s) \approx 1$ in the latter limit, the histogram $h_2(s)$ is given (up to a known prefactor) by $s^{d+1}u_{\rm s}'(s)$. As one expects, the decay is faster for the $d = 2$ data than for the KA mixtures in $d = 3$ since the phase volume at the cutoff is larger for the latter systems. Since all histograms are rather smooth, one may simply set $s = s_{\rm c}$ for obtaining $\Delta\mu_{\rm B}$ from $h_2(s)$ instead of properly taking the limit $s \to s_{\rm c}^-$.

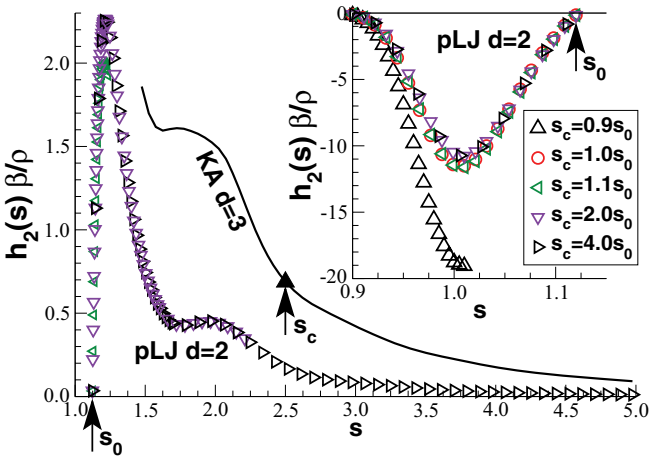

FIG. 1. (Color online) Weighted radial pair distribution function $h_2(s)\beta/\rho$ with $s = r/\sigma_l$ being the reduced distance between two beads i and j. Main panel: KA mixtures in $d = 3$ (bold line) and pLJ beads in $d = 2$ (open symbols) for large reduced distances $s > s_0$ where the potential is attractive. The filled triangle corresponds to the shear modulus $\tilde{G}$ computed using Eq. (20) for the KA system not taking into account the impulsive correction. Inset: pLJ model for $s \leqslant s_0$ where $h_2(s)$ becomes strongly negative.

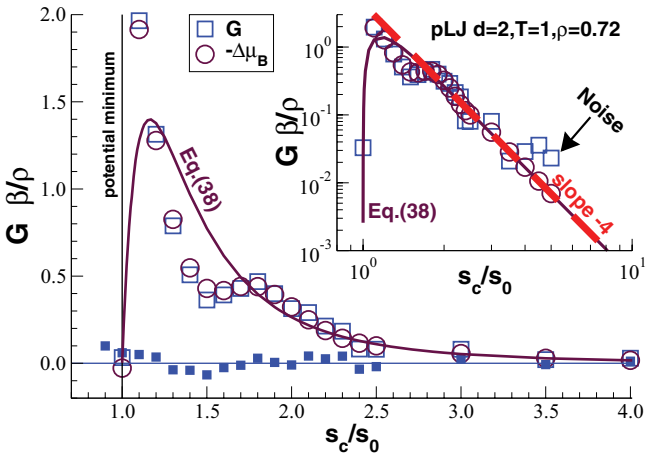

FIG. 2. (Color online) Shear modulus G and impulsive correction $-\Delta\mu_B$ for the pLJ model vs the reduced cutoff distance s_c/s_0. The uncorrected shear modulus $\tilde{G}$ (open squares) has been obtained using the stress-fluctuation formula (20), and the correction term (spheres) from the histogram $h_2(s)$, Eq. (18). The solid lines indicate Eq. (38) where we have set $g_{tt'}(s_c) = 1$. Main panel: linear representation showing that $G = \tilde{G} + \Delta\mu_B$ (filled squares) vanishes as predicted [Eq. (27)]. Inset: double-logarithmic representation emphasizing the asymptotic power-law decay for large s_c [Eq. (35)], as indicated by the bold dashed line.

B. Compression modulus K

The compression modulus K may be obtained from Eq. (19) or, equivalently, using the Rowlinson formula (21) [39]. All our systems are highly incompressible, i.e., the compression modulus K is large as usual in condensed matter systems, and it is thus difficult to demonstrate the small correction predicted by Eq. (26). For the KA model, we obtain, e.g., $\Delta K\beta/\rho \approx -(5/4) \times 0.69 \approx -1.2$, which compared to the uncorrected estimate $\tilde{K}\beta/\rho \approx 21.9$ is small.

More importantly, it is not easy to obtain an independent and precise K value for canonical ensembles of mixtures and polydisperse systems using, e.g., the total particle structure factor [19,33]. For the pLJ model, we have thus computed K directly from the volume fluctuations δV in the isobaric ensemble [1]

$$K = k_B T \frac{\langle V \rangle}{\langle \delta^2 V \rangle}, \tag{39}$$

where we impose the same (mean) pressure P as for the corresponding canonical ensemble. As described in Ref. [1], proposed volume fluctuations of the simulation box are accepted or rejected according to a METROPOLIS MC scheme. As may be seen from the last column indicated in Table I, this yields within statistical accuracy the same values as the stress-fluctuation formula (19), if the impulsion correction is taken into account. Unfortunately, for larger cutoffs, our error bars (not shown) become too large to confirm the correction. The most striking example, where Eq. (26) can be shown to work, is the case of the small cutoff $s_c = 0.9s_0$: Using Eq. (19), an impossible *negative* value $\tilde{K}\beta/\rho \approx -20.4$ is obtained. As may be seen from the inset in Fig. 1, one gets $\Delta\mu_B\beta/\rho \approx 19.1$ from the weighted histogram $h_2(s)$. Taking the correction (26) into account, this yields $K\beta/\rho \approx 17.7$, which is consistent with the value 17.4 obtained using the strain fluctuation formula (39).

C. Shear modulus G

Asymptotic limit for large sampling times. Since all our systems are liquids, the shear modulus G should of course vanish, at least in the thermodynamic limit for a sufficiently long sampling time. We have thus a clear reference and for this reason G is highly suitable to test our predictions. As can be seen from the solid triangle indicated in Fig. 1 for the KA mixtures with $s_c = 2.5$, we obtain $\tilde{G}\beta/\rho \approx 0.65$ if the impulsive correction for the Born term is *not* taken into account. As also shown by the figure (thin line), this deviation equals $h_2(s_c = 2.5)\beta/\rho \approx 0.69$ as predicted.

The same behavior is seen from Fig. 2 for pLJ beads for a broad range of cutoff distances s_c where the open squares refer to the uncorrected $\tilde{G}$ and the filled squares to G obtained using Eq. (27). The solid lines indicated show Eq. (38). Focusing on the scaling for large s_c, we have set $g_{tt'}(s_c) = 1$ in the double integral which (under this assumption) is close to unity. Note that the correction $-\Delta\mu_B$ (open spheres) is obtained with much higher numerical precision than it was possible for $\tilde{G}$. The error bars (not indicated) become larger than the signal below $\tilde{G}\beta/\rho \approx 0.05$.

Sampling time dependence. Figure 3 gives additional information on the shear modulus $G(t)$ plotted as a function of the number t of MC steps (MCS) for pLJ beads. Using time series where instantaneous properties relevant for the moments are written down every 10 MCS for total trajectories of length 10^7 MCS, all reported properties have been averaged using standard gliding averages [1], i.e., we compute mean values and fluctuations for a given time interval $[t_0, t_1 = t_0 + t]$ and average over all possible intervals of length t. For $s_c = 0.9s_0$, where $\Delta\mu_B\beta/\rho \approx 17.1$, the uncorrected data is negative and can not be represented. Note that $G = \tilde{G}$ for $s_c = 1.0s_0$ since $\Delta\mu_B = 0$ for $s_c = 1.0s_0$ [Eq. (18)]. Since $\Delta\mu_B$ is very small

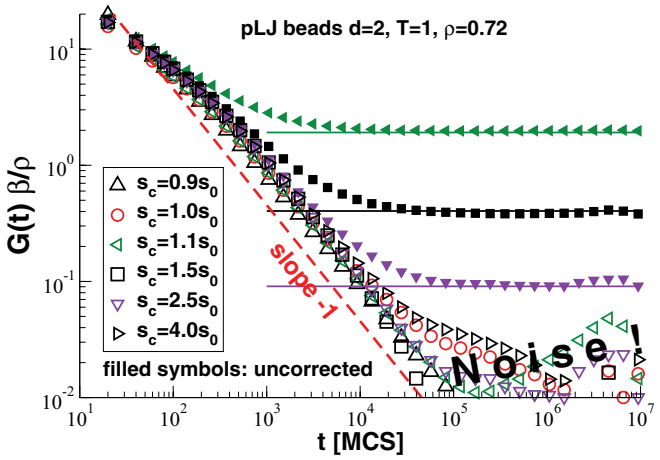

FIG. 3. (Color online) Shear modulus G for pLJ beads in $d = 2$ for different s_c as a function of the sampling time t given in units of MC steps (MCS) of the local MC jumps used. The vertical axis is made dimensionless by means of a factor β/ρ. Filled symbols refer to the uncorrected $\tilde{G}(t)$. The horizontal lines indicate $-\Delta\mu_B$ obtained from the histograms $h_2(s)$ for three cutoffs as indicated in the Table I. The dashed slope characterizes the decay of (the corrected) $G(t)$ with time.

for $s_c = 4.0s_0$, only the corrected values are represented. The filled symbols refer to the uncorrected shear modulus $\tilde{G}(t)$ for $s_c = 1.1s_0$, $1.5s_0$, and $2.5s_0$, which are seen to approach for large times the predicted correction $-\Delta\mu_B$ taken from the Table I (horizontal lines). If corrected, all data sets vanish properly with time. [The noise becomes again too large below $G(t)\beta/\rho \approx 0.05$.]

Interestingly, neither μ_B nor P_{ex} do (essentially) depend on the sampling time t, while the fluctuation contribution $-\mu_F(t)$ approaches (the corrected) $\mu_B - P_{ex}$ from below (not shown). The corrected shear modulus $G(t)$ thus decreases monotonously with time. As can be seen from Fig. 3, $G(t)$ decays roughly as the power-law slope -1 indicated by the dashed line. Exactly the same behavior has been observed for the KA model in $d = 3$ (not shown). Apparently, $G(t)$ decays quite generally inversely as the mean-square displacement $h(t)$ of the beads in the free-diffusion limit $h(t) \sim t$. We remind that the same scaling $G(t) \sim 1/h(t)$ has also been reported for a bead-spring polymer model without impulsive corrections ($s_c = s_0$) [19].

V. DISCUSSION

A. Summary

Impulsive correction. We have emphasized in this study that an impulsive correction to the Born contribution $C_B^{\alpha\beta\gamma\delta}$ of the elastic moduli must arise if the interaction potential is truncated and shifted [Eq. (3)], with a nonvanishing first derivative at the cutoff. To test our theoretical predictions, we have computed the elastic moduli of isotropic liquids in $d = 3$ and 2 dimensions. Since for these systems the shear modulus G must vanish by construction, this allows a precise numerical verification for different reduced cutoff distances s_c (Fig. 2). It has been shown how the impulsive correction for mixtures and polydisperse systems may be obtained from the weighted histogram $h_2(s)$ which scales as $h_2(s) \sim s^{d+1}u'(s)$ for large s. As one expects, the cutoff effect vanishes if s_c is large [Eq. (35)] or set to the minimum of the potential. It becomes more important with increasing spatial dimension.

General validity of the stress-fluctuation formalism. It should be reminded that the stress-fluctuation formula $G = \mu - P = \mu_B + \mu_F - P_{ex}$ and several other relations used in this work for *liquid* systems were originally formulated for *solids* assuming well-defined reference positions and displacement fields [8,16]. By revisiting the derivation [6] for the compression modulus K for simple liquids [Eq. (21)] for general elastic moduli (as in fact already done by Lutsko [12]), it can be seen that these assumptions can be relaxed and especially Eq. (20) must hold quite generally for isotropic systems [34]. One additional goal of the present paper was to show numerically that the stress-fluctuation formalism yields the right value ($G = 0$), *once* the impulsive correction has been taken into account.

B. Further generalizations and related issues

The generalization of our results to

(i) other elastic moduli in anisotropic systems using the more general impulsive correction [Eq. (11)];

(ii) observables related to even higher derivatives of the potential [Eq. (13)];

(iii) local and inhomogeneous elastic moduli which have been argued to be of relevance for the plastic failure under external load [14,16,17];

(iv) more complicated interaction potentials, not necessarily scaling simply with $s = r/\sigma_l$;

(v) general nonpair interactions using the generalization of the Born term derived by Ray [10] and studied, e.g., numerically by Yoshimoto *et al.* [15]

is straightforward and should be considered in the future [40].

C. Shear modulus near the glass transition

We are currently using the presented approach to characterize as a function of temperature, imposed pressure, and sampling time the elastic properties of the two models presented here [34]. Preliminary results are shown in Fig. 4. Following the procedure described in Ref. [18], the data have been obtained for systems which are cooled through the glass transition at constant pressure P, i.e., allowing first the volume to fluctuate as in Sec. IV B [36,41]. The glass transition temperature T_g of both systems is either known [31] or may be determined, e.g., from the density $\rho(T)$ [18]. Imposing then a constant (mean) temperature and a simulation box of fixed volume and shape, the shear modulus is computed using the stress-fluctuation formula (20) for the canonical ensemble. The bare moduli $\tilde{G}$ (open squares and triangles) are clearly seen to be finite for all T, while the corrected moduli $G = \tilde{G} + \Delta\mu_B$ vanish for all $T > T_g$. That this is indeed the case is better seen from the half-logarithmic representation shown in the inset for the KA model. Decreasing the temperature further below T_g, the shear moduli are seen to increase rapidly for both models [42]. As above for the compressibility K in Sec. IV B, we have crosschecked the values obtained from the stress fluctuations in

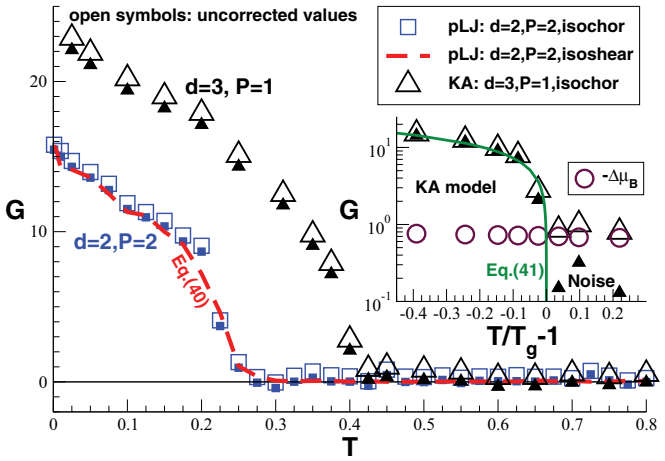

FIG. 4. (Color online) Shear modulus G as a function of temperature T for the KA model ($P \approx 1$, $s_c = 2.5$, $T_g \approx 0.41$) and the pLJ model ($P \approx 2$, $s_c = 2.0s_0$, $T_g \approx 0.27$). The uncorrected values are represented by open symbols, the corrected values by small filled symbols. Main panel: the dashed line represents the shear modulus obtained from the shear strain fluctuations in simulation boxes with shape deformations, Eq. (40). Inset: half-logarithmic representation for $G(T)$ for the KA model focusing on the behavior around T_g. The transition becomes rather sharp if the impulsive correction is taken into account as emphasized by the solid line indicating Eq. (41). Note that $-\Delta\mu_B$ (spheres) increases only weakly with decreasing T.

the canonical ensemble by directly measuring G from the shear strain γ (in the xy plane) in deformable simulation boxes at constant volume. As discussed in the literature [1,2,16], we use a non-Euclidean metric tensor constructed from the so-called h matrix describing the box shape, and change the shear strain γ according to a METROPOLIS MC scheme [1] similar to the changes of the box volume V in Sec. IV B. By imposing a zero mean shear stress for the shear strain fluctuations, the modulus G can be obtained from the thermodynamic formula

$$G = \frac{k_B T / V}{\langle \gamma^2 \rangle - \langle \gamma \rangle^2}, \tag{40}$$

which corresponds to Eq. (39) for volume fluctuations in the isobaric ensemble [43]. As shown for the pLJ model by the dashed line in the main panel of Fig. 4, this yields for all T, even for deeply quenched glasses, within numerical accuracy the *same* values as the stress-fluctuation formula *if* the impulsive corrections are taken into account. As shown by the solid line in the inset, the KA model is well fitted by a cusp singularity

$$G(T) \approx G_0(1 - T/T_g)^{1/2} \text{for} T < T_g \tag{41}$$

with an empirical constant $G_0 \approx 23$. This suggests that the transition is very sharp albeit continuous in agreement with replica theory [22,24]. Note that the number of data points close to T_g is, however, not sufficient to rule out completely the additive offset suggested by MCT [21,25]. Thus, at present we can not distinguish between different theoretical scenarios proposed [21–25]. If a similar relation as Eq. (41) holds for our two-dimensional model is currently also an open question. (Especially, the latter systems need to be recomputed with MD and sampling time effects have to be considered more carefully.) In any case, it should be clear from Fig. 4 that a high-precision numerical characterization of the scaling of $G(T)$ around T_g necessitates the proper taking into account of the impulsive corrections.

ACKNOWLEDGMENTS

H.X. thanks the CNRS and the IRTG Soft Matter for supporting her sabbatical stay in Strasbourg and P.P. thanks the Région Alsace and the IRTG Soft Matter for financial support. We are indebted to H. Meyer, O. Benzerara, and J. Farago (all ICS, Strasbourg) for helpful discussions.

[1] M. Allen and D. Tildesley, *Computer Simulation of Liquids* (Oxford University Press, Oxford, 1994).
[2] D. Frenkel and B. Smit, *Understanding Molecular Simulation–From Algorithms to Applications*, 2nd ed. (Academic, San Diego, 2002).
[3] J. Thijssen, *Computational Physics* (Cambridge University Press, Cambridge, 1999).
[4] S. Toxvaerd and J. C. Dyre, J. Chem. Phys. **134**, 081102 (2011).
[5] M. Abramowitz and I. A. Stegun, *Handbook of Mathematical Functions* (Dover, New York, 1964).
[6] J. S. Rowlinson, *Liquids and Liquid Mixtures* (Butterworths Scientific Publications, London, 1959).
[7] D. C. Wallace, in *Solid State Physics: Advances in Research and Applications*, edited by H. Ehrenreich, F. Seitz, and D. Turnbull, Vol. 25 (Academic, New York, 1970), p. 300.
[8] D. R. Squire, A. C. Holt, and W. G. Hoover, Physica (Amsterdam) **42**, 388 (1969).
[9] J. R. Ray and A. Rahman, J. Chem. Phys. **80**, 4423 (1984).
[10] J. R. Ray, Comput. Phys. Rep. **8**, 109 (1988).
[11] J. F. Lutsko, J. Appl. Phys. **64**, 1152 (1988).
[12] J. F. Lutsko, J. Appl. Phys. **65**, 2991 (1989).
[13] C. Maloney and A. Lemaître, Phys. Rev. Lett. **93**, 195501 (2004).
[14] K. Yoshimoto, T. S. Jain, K. Van Workum, P. F. Nealey, and J. J. de Pablo, Phys. Rev. Lett. **93**, 175501 (2004).
[15] K. Yoshimoto, G. J. Papakonstantopoulos, J. F. Lutsko, and J. J. de Pablo, Phys. Rev. B **71**, 184108 (2005).
[16] J.-L. Barrat, in *Computer Simulations in Condensed Matter Systems: From Materials to Chemical Biology*, edited by M. Ferrario, G. Ciccotti, and K. Binder, Vol. 704 (Springer, Berlin, 2006), pp. 287–307.
[17] M. Tsamados, A. Tanguy, C. Goldenberg, and J.-L. Barrat, Phys. Rev. E **80**, 026112 (2009).
[18] B. Schnell, H. Meyer, C. Fond, J. Wittmer, and J. Baschnagel, Eur. Phys. J. E **34**, 97 (2011).
[19] N. Schulmann, H. Xu, H. Meyer, P. Polińska, J. Baschnagel, and J. P. Wittmer, Eur. Phys. J. E **35**, 93 (2012).
[20] S. Ulrich, X. Mao, P. Goldbart, and A. Zippelius, Europhys. Lett. **76**, 677 (2006).

[21] W. Götze, *Complex Dynamics of Glass-Forming Liquids: A Mode-Coupling Theory* (Oxford University Press, Oxford, 2009).
[22] H. Yoshino and M. Mézard, Phys. Rev. Lett. **105**, 015504 (2010).
[23] G. Szamel and E. Flenner, Phys. Rev. Lett. **107**, 105505 (2011).
[24] H. Yoshino, J. Chem. Phys. **136**, 214108 (2012).
[25] C. L. Klix, F. Ebert, F. Weysser, M. Fuchs, G. Maret, and P. Keim, Phys. Rev. Lett. **109**, 178301 (2012).
[26] G. Parisi and F. Zamponi, Rev. Mod. Phys. **82**, 789 (2010).
[27] E. del Gado and W. Kob, J. Non-Newtonian Fluid Mech. **149**, 28 (2008).
[28] C. Tonhauser, D. Wilms, Y. Korth, H. Frey, and C. Friedrich, Macromol. Rapid Commun. **31**, 2127 (2010).
[29] M. Filali, M. J. Ouazzani, E. Michel, R. Aznar, G. Porte, and J. Appell, J. Phys. Chem. B **105**, 10528 (2001).
[30] A. Zilman, J. Kieffer, F. Molino, G. Porte, and S. A. Safran, Phys. Rev. Lett. **91**, 015901 (2003).
[31] W. Kob and H. C. Andersen, Phys. Rev. E **52**, 4134 (1995).
[32] A. Tanguy, J. P. Wittmer, F. Leonforte, and J.-L. Barrat, Phys. Rev. B **66**, 174205 (2002).
[33] J. Hansen and I. McDonald, *Theory of Simple Liquids* (Academic, New York, 1986).
[34] H. Xu, P. Polińska, J. Baschnagel, and J. P. Wittmer (unpublished).
[35] Apart from the Born term $C_{\mathrm{B}}^{\alpha\beta\gamma\delta}$ and the stress-fluctuation term $C_{\mathrm{F}}^{\alpha\beta\gamma\delta}$, there is a kinetic contribution $C_{\mathrm{K}}^{\alpha\beta\gamma\delta}$ and in prestressed systems (as in the systems considered numerically by us) an explicit contribution from the applied stress to the experimentally relevant elastic moduli resulting from an infinitesimal strain applied to the reference state [2,7,18].
[36] For systems with finite mean shear stress, various stress-fluctuation formulas must be changed and especially Eq. (20) for the shear modulus G must be modified.
[37] The trivial kinetic energy contributions to the elastic moduli are removed as far as possible from the presentation since MC results are also considered here.
[38] F. Birch, J. Appl. Phys. **9**, 279 (1938).
[39] If plotted as a function of the number of configurations sampled, the compression modulus for both models is seen to decrease first with sampling time t before leveling off at a finite value. Similar behavior has been observed for polymeric systems [18,19].
[40] A similar, albeit very small, impulsive correction arises for the "configurational temperature" being the ratio of the mean-squared forces acting on the particles and the mean divergence of these forces. See Eq. (7.2.11) of Ref. [33].
[41] For our low-temperature MC simulations, we use in addition to the standard local jump moves both longitudinal and (more importantly) transverse plane waves with wave vectors commensurate with the simulation box. The amplitudes of the collective displacement fields for each wave vector are chosen as implied by continuum theory. If such collective displacements are included, the shear stress for one given quenched configuration can be shown to be negligible as required [36].
[42] It is well known that two-point correlations, as measured by the pair correlation function $g(r)$, do barely change at the glass transition [21]. Please note that the shear modulus G computed according to Eq. (20) is a properly defined thermodynamic correlation function characterizing not only two-point, but also three- and four-point correlations. Apparently, these higher *static* correlations change qualitatively at the glass transition.
[43] Since such a thermodynamic relation may be questioned for the strongly frozen systems, we have also determined G using the mechanical definition by linear regression from the observed conjugated instantaneous shear strain and stress. This yields the *same* values as Eq. (40).